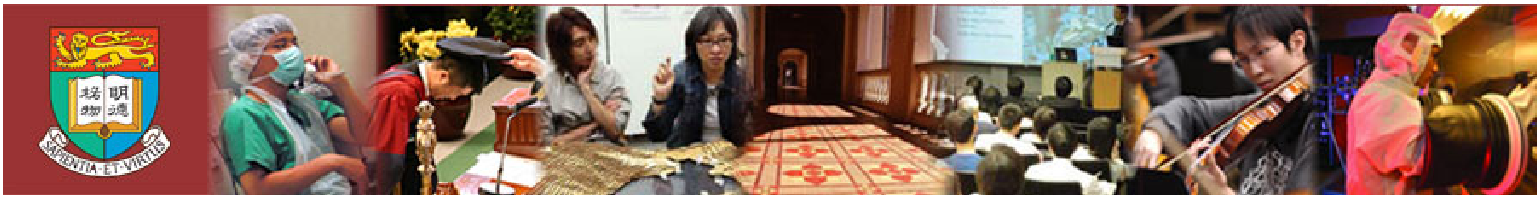

Title	Performance analysis and design of FxLMS algorithm in broadband ANC system with online secondary-path modeling
Author(s)	Chan, SC; Chu, Y
Citation	IEEE Transactions on Audio, Speech and Language Processing, 2012, v. 20 n. 3, p. 982-993
Issued Date	2012
URL	http://hdl.handle.net/10722/139284
Rights	©2012 IEEE. Personal use of this material is permitted. However, permission to reprint/republish this material for advertising or promotional purposes or for creating new collective works for resale or redistribution to servers or lists, or to reuse any copyrighted component of this work in other works must be obtained from the IEEE.

Performance Analysis and Design of FxLMS Algorithm in Broadband ANC System With Online Secondary-Path Modeling

Shing-Chow Chan and Yijing Chu

***Abstract*—The filtered-x LMS (FxLMS) algorithm has been widely used in active noise control (ANC) systems, where the secondary path is usually estimated online by injecting auxiliary noises. In such an ANC system, the ANC controller and the secondary-path estimator are coupled with each other, which make it difficult to analyze the performance of the entire system. Therefore, a comprehensive performance analysis of broadband ANC systems is not available currently to our best knowledge. In this paper, the convergence behavior of the FxLMS algorithm in broadband ANC systems with online secondary-path modeling is studied. Difference equations which describe the mean and mean square convergence behaviors of the adaptive algorithms are derived. Using these difference equations, the stability of the system is analyzed. Finally, the coupled equations at the steady state are solved to obtain the steady-state excess mean square errors (EMSEs) for the ANC controller and the secondary-path estimator. Computer simulations are conducted to verify the agreement between the simulated and theoretically predicted results. Moreover, using the proposed theoretical analysis, a systematic and simple design procedure for ANC systems is proposed. The usefulness of the theoretical results and design procedure is demonstrated by means of a design example.**

***Index Terms*—Active noise control (ANC), design, filtered-x LMS (FxLMS), online secondary-path modeling, performance analysis.**

I. Introduction

ACTIVE noise control (ANC) systems [1]–[3] are frequently employed to reduce undesired noise sound in headsets, industrial ducts, automobiles, etc. Compared with other passive methods, ANC offers more flexibility in controlling low-frequency noises. One of the most widely used adaptive control algorithms for ANC systems is the filtered-x LMS (FxLMS) algorithm [4], [5]. An important issue in the FxLMS algorithm is the modeling of the secondary path. In the simplest case, the secondary path is assumed to be known or estimated offline using system identification techniques. Recently, more attention has been paid to online secondary-path modeling so as to combat the modeling errors and other variations or uncertainties encountered in practical situations [6]–[12]. The well-known structure in [6] with auxiliary noise injection is commonly employed, where the secondary path is identified online during the operation of the ANC controller.

The performance of the ANC system is affected both by the ANC controller and the secondary-path estimator. More precisely, the filtered input of the ANC controller is determined by the secondary-path modeling. On the other hand, the accuracy of the secondary-path modeling depends on the residue of the controller. Hence, the performance analysis of such an ANC system becomes very difficult due to the interaction or coupling of the two adaptive systems. For narrowband ANC systems with online secondary-path modeling, a comprehensive theoretical analysis was recently carried out in [13] and [14]. In [13], the difference equations governing the dynamics of the entire system were developed and the steady-state estimation of mean square errors (MSEs) of both the ANC controller and the secondary-path estimator were derived in a closed form. Similar work was conducted for the narrowband ANC system with scaled auxiliary noise [14].

For broadband ANC systems, factors affecting the system performance were studied in [15]. The convergence behavior of the aforementioned methods in [7]–[10] was also compared and evaluated preliminarily through statistical analysis, which provides useful guidance to the design of broadband systems. However, to our best knowledge, a detailed performance analysis on important issues such as convergence rate, steady-state excess mean square error (EMSE) over the ideal Wiener filter, and maximum step-sizes to achieve stability is unavailable. Driven by the practical advantages of broadband ANC systems, the present paper is devoted to bridge this gap in the literature of broadband ANC systems.

In particular, we conduct a detailed performance analysis of broadband ANC systems with online secondary-path modeling for Gaussian inputs and additive noises. The difference equations describing the mean and mean square convergence behaviors of the FxLMS algorithm for the ANC controller and the LMS algorithm for online secondary-path modeling are derived. The Wiener solutions are derived from these difference equations and it is found that a modeling error may exist between the Wiener solution and the true solution if the filter length is insufficient. The difference equations also characterize the coupling between the controller and the secondary-path estimator. Using the difference equations of the coupled adaptive systems, the convergence conditions are discussed. Finally, the decoupled equations at the steady state are solved to obtain formulas of the EMSE for the ANC controller and the secondary-path

Manuscript received March 23, 2011; revised July 20, 2011; accepted September 02, 2011. Date of publication September 29, 2011; date of current version January 25, 2012. The associate editor coordinating the review of this manuscript and approving it for publication was Prof. Boaz Rafaely.

The authors are with The University of Hong Kong, Hong Kong, SAR(e-mail: scchan@eee.hku.hk; yjchu@eee.hku.hk).

Digital Object Identifier 10.1109/TASL.2011.2169789

estimator. Consequently, useful guidelines for step-size selection to achieve a given EMSE can be provided. This provides valuable insight and possible guidance for future ANC system design. Computer simulations show that the theoretical analyses can satisfactorily predict the convergence behaviors of the ANC systems and can lead to the proposed design procedure for ANC systems.

The rest of the paper is organized as follows. In Section II, the ANC system is briefly introduced. Section III is devoted to the mean and mean square convergence performance analyses of the above system. Simulation results and comparison with the theoretical analyses will be presented in Section IV. Finally, a conclusion is drawn in Section V.

II. ANC System With Online Secondary-Path Modeling

Consider the ANC system with online secondary-path modeling in Fig. 1, where the undesirable acoustic signal generated from a source S at location E is to be minimized by the acoustic signal generated from a loudspeaker A through an appropriate excitation using an adaptive filter-based controller $\{w_k(n)\}$. An error microphone at E is used to pick up the residual signal $e(n)$ at time instant n to be minimized. The acoustic path from S to E, called the primary path, is modeled as a discrete time linear system with impulse response $\{p_k(n)\}$, $k = 0, \ldots$. Similarly, the acoustic path from A to E, called the secondary path, is modeled as $\{s_k(n)\}$ and it is estimated online using an adaptive filter $\{\hat{s}_k(n)\}$ by injecting an auxiliary noise $\{g(n)\}$ at A. For time-invariant channels, $\{p_k(n)\}$ and $\{s_k(n)\}$ will be independent of the time index n. The ANC controller $\{w_k(n)\}$ approximates $\{-p_k(n)\}$ after cascading with $\{s_k(n)\}$ so that the undesirable contribution from the noise source to location E is minimized. $\{w_k(n)\}$ is usually chosen as a finite duration impulse (FIR) filter, say with length L_w : $\boldsymbol{w}(n) = [w_1(n), w_2(n), \ldots, w_{L_w}(n)]^T$, which can be updated using variants of the LMS algorithm, called the FxLMS-based algorithms. More precisely, we can see from Fig. 1 that the contribution of $x(n)$ at E is $p_k(n) * x(n)$, and the contribution of the loudspeaker at E is $-y(n) = y_{\hat{w}}(n) + y_s(n)$, where $y_{\hat{w}}(n) = x(n) * w_k(n) * s_k(n)$, $y_s(n) = g(n) * s_k(n)$, and the symbol "$*$" stands for the discrete time convolution. Let $\eta(n)$ be the background noise and other acoustic signals at E, then

$$e(n) = d(n) - y(n) \tag{1}$$

where $d(n) = p_k(n) * x(n) + \eta(n)$. The mean squares error of $e(n)$ can be minimized by the well-known LMS algorithm with desired input $d(n)$ and output $y_{\hat{w}}(n)$. Since the discrete-time convolution is commutative, the equivalent input of the adaptive filter should be $x_s(n) = x(n) * s_k(n)$. However, since $\{s_k(n)\}$ is unknown, it is replaced by its estimated value $\{\hat{s}_k(n)\}$ and the input to the adaptive filter is $\hat{x}_s(n) = x(n) * \hat{s}_k(n)$. This gives the following update equations for the ANC system:

$$e_s(n) = e(n) - y_{\hat{s}}(n) \tag{2}$$
$$\boldsymbol{w}(n+1) = \boldsymbol{w}(n) - \mu_w e(n)\hat{\boldsymbol{x}}_s(n) \tag{3}$$
$$\hat{\boldsymbol{s}}(n+1) = \hat{\boldsymbol{s}}(n) + \mu_s e_s(n)\boldsymbol{g}(n) \tag{4}$$

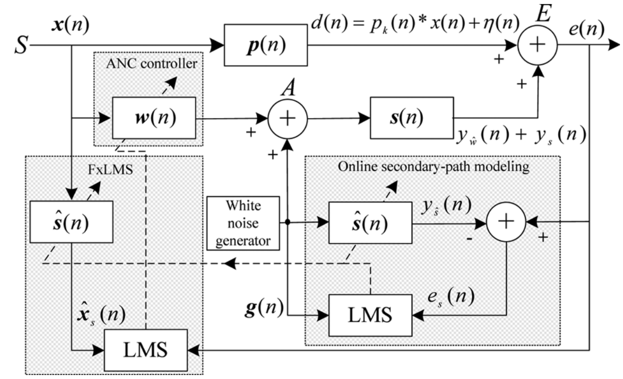

Fig. 1. ANC system with online secondary-path modeling.

where $\hat{\boldsymbol{x}}_s(n) = [\hat{x}_s(n), \hat{x}_s(n-1), \ldots, \hat{x}_s(n-L_w+1)]^T$, μ_w and μ_s are, respectively, the step-sizes for updating $\boldsymbol{w}(n)$ and $\{\hat{s}_k(n)\}$, which is chosen as an $L_{\hat{s}}$-tap adaptive filter $\hat{\boldsymbol{s}}(n) = [\hat{s}_1(n), \hat{s}_2(n), \ldots, \hat{s}_{L_{\hat{s}}}(n)]^T$, $\boldsymbol{g}(n) = [g(n), g(n-1), \ldots, g(n-L_{\hat{s}}+1)]^T$, and $y_{\hat{s}}(n) = \hat{s}^T(n)g(n)$. Since $\{x(n)\}$ is filtered by $\{\hat{s}_k(n)\}$ in (3), the algorithm is called the FxLMS algorithm.

In this paper, we shall study the convergence performance of the above ANC system using the conventional FxLMS algorithm and the LMS algorithm. The analytical approach to be presented is sufficiently general to be extended to other adaptive filter algorithms.

III. Performance Analysis

In this section, the convergence performance analysis of the FxLMS algorithm with online secondary-path modeling given by (1)–(4) will be studied. The difference equations describing the mean and mean square behaviors of this system and the steady-state EMSE will be derived. To simplify the analysis, the following assumptions will be used.

(A1) The input $\boldsymbol{x}_L(n) = [x(n), x(n-1), \ldots, x(n-L+1))]^T$ is an independent identically distributed (i.i.d.) Gaussian random sequence with zero-mean and covariance $\boldsymbol{R}_{xx}$.

(A2) The auxiliary noise $\{g(n)\}$ is Gaussian-distributed with zero-mean and covariance $\boldsymbol{R}_{gg}$ and the background white Gaussian noise $\{\eta(n)\}$ is zero mean with variance σ_η^2. $\{\boldsymbol{x}(n)\}$, $\{g(n)\}$ and $\{\eta(n)\}$ are independent with each other.

(A3) The weight vector $\boldsymbol{w}(n)$ and $\hat{\boldsymbol{s}}(n)$ are independent with $\{x(n)\}$ and $\{g(n)\}$, which is the widely used independence assumption [16].

(A4) The primary and secondary paths are assumed to be linear shift invariant filters of finite duration, i.e., $\boldsymbol{p} = [p_0, p_1, \ldots, p_{L_p-1}]^T$ and $\boldsymbol{s} = [s_0, s_1, \ldots, s_{L_s-1}]^T$.

From (A1)(A4) and Fig. 1, we have: $d(n) = \boldsymbol{p}^T\boldsymbol{x}_{L_p}(n) + \eta(n)$, $-y(n) = \boldsymbol{w}^T(n)\boldsymbol{x}_s(n) + \boldsymbol{s}^T\tilde{\boldsymbol{g}}(n)$, where $\boldsymbol{x}_s(n) = [x_s(n), x_s(n-1), \ldots, x_s(n-L_w+1)]^T$ and $\tilde{\boldsymbol{g}}(n) = [g(n), g(n-1), \ldots, g(n-L_s+1)]^T$. Hence,

$$e(n) = d(n) + \boldsymbol{w}^T(n)\boldsymbol{x}_s(n) + \boldsymbol{s}^T\tilde{\boldsymbol{g}}(n) \tag{5}$$
$$\begin{aligned} e_s(n) &= e(n) - y_{\hat{s}}(n) \\ &= d(n) + \boldsymbol{w}^T(n)\boldsymbol{x}_s(n) + \boldsymbol{s}^T\tilde{\boldsymbol{g}}(n) - \hat{\boldsymbol{s}}^T(n)\boldsymbol{g}(n). \end{aligned} \tag{6}$$

A. Mean Convergence Analysis

We shall analyze the mean convergence performance of the secondary-path adaptive filter and the FxLMS algorithm-based ANC controller in turn.

1) Secondary-Path Adaptive Filter: First of all, we note that the Wiener solution to $\hat{\boldsymbol{s}}(n)$ is

$$\boldsymbol{s}^* = \boldsymbol{R}_{gg}^{-1} E[\boldsymbol{g}(n)\tilde{\boldsymbol{g}}(n)^T]\boldsymbol{s}. \tag{7}$$

It can be seen that for $L_{\hat{s}} \geq L_s$, $\boldsymbol{s}^* = \boldsymbol{s}$. Otherwise, a modeling error will exist. Consequently, $\hat{\boldsymbol{x}}_s(n) \overset{n \text{ large}}{\longrightarrow} \boldsymbol{x}_s(n)$ and hence all the cross-correlation matrices of the form $\boldsymbol{R}_{\hat{x}_s x_s}$ will be asymptotic symmetric. As we shall see later, this considerably simplifies the mean and mean squares convergence analyses. Therefore, for simplicity, we shall assume in the sequel that $L_{\hat{s}} = L_s$, and hence $\boldsymbol{g}(n) = \tilde{\boldsymbol{g}}(n)$ and $\boldsymbol{s}^* = \boldsymbol{s}$. A possible limitation is that a longer adaptive filter may be used to ensure that the performance predicted by the analysis is reasonably accurate. Fortunately, from the simulation results to be presented later in Section IV-B, we found that the theoretical analysis is not so sensitive to possible channel length mismatches.

Let the weight error vector be $\boldsymbol{\nu}_s(n) = \boldsymbol{s} - \hat{\boldsymbol{s}}(n)$ and taking expectation on both sides of (4), one gets

$$\begin{aligned}\bar{\boldsymbol{\nu}}_s(n+1) &= \bar{\boldsymbol{\nu}}_s(n) - \mu_s E[(e_0(n) + \boldsymbol{\nu}_s^T(n)\boldsymbol{g}(n))\boldsymbol{g}(n)] \\ &= (\boldsymbol{I} - \mu_s \boldsymbol{R}_{gg})\bar{\boldsymbol{\nu}}_s(n)\end{aligned} \tag{8}$$

where $\bar{\boldsymbol{\nu}}_s(n) = E[\boldsymbol{\nu}_s(n)]$ and $e_0(n) = d(n) + \boldsymbol{w}^T(n)\boldsymbol{x}_s(n)$. Note that $e_0(n)$ is independent of $\boldsymbol{g}(n)$. It can be seen from (8) that the mean weight vector $E[\hat{\boldsymbol{s}}(n)]$ will converge to its Wiener solution $\boldsymbol{s}^* = \boldsymbol{s}$, if the step-size satisfies $|1 - \mu_s \lambda_{g,\max}| < 1$ or equivalently $0 < \mu_s < 2/\lambda_{g,\max}$, where $\lambda_{g,\max}$ is the maximum eigenvalue of $\boldsymbol{R}_{gg}$. It can be seen the convergence speed for a given step-size is the fastest when the injection $\{g(n)\}$ is white since all eigenvalues of $\boldsymbol{R}_{gg}$ are identical and of equal power, i.e., σ_g^2. To avoid unnecessary complications, we only consider the case where $\{g(n)\}$ is white in subsequent sections. Consequently, the step-size has to satisfy $0 < \mu_s < 2/\sigma_g^2$ and a larger step-size or larger noise power σ_g^2 will lead to a faster convergence rate [11]. However, the auxiliary noise is expected to be as small as possible in order to reduce the interference noise to the ANC controller at E. Two solutions to the problem are 1) to vary the auxiliary noise power according to the residual noise power [11], [21] and 2) to use a variable step-size algorithm to obtain a fast convergence rate and low MSE as in [17].

2) FxLMS ANC Controller: For the ANC controller, we shall assume that the algorithm converges so as to derive its steady-state solution $\boldsymbol{w}^*$. Later, we shall determine the condition for convergence. At the steady state, we have from (3) that $E[e(n)\hat{\boldsymbol{x}}_s(n)] = E[(\boldsymbol{x}_{L_p}^T(n)\boldsymbol{p} + \boldsymbol{x}_s^T(n)\boldsymbol{w}^*(n) + \boldsymbol{g}^T(n)\boldsymbol{s})\hat{\boldsymbol{x}}_s(n)] = 0$, which gives

$$\boldsymbol{R}_{\hat{x}_s x_s}(n)\boldsymbol{w}^*(n) = -\boldsymbol{r}_{\hat{x}_s x}(n)\boldsymbol{p} \tag{9}$$

where $\boldsymbol{R}_{\hat{x}_s x_s}(n) = E[\hat{\boldsymbol{x}}_s(n)\boldsymbol{x}_s^T(n)]$ and $\boldsymbol{r}_{\hat{x}_s x_s}(n) = E[\hat{\boldsymbol{x}}_s(n)\boldsymbol{x}_{L_p}^T(n)]$. To evaluate the expectations, we note that $\hat{\boldsymbol{x}}_s(n) = [\boldsymbol{x}_{L_{\hat{s}}}^T(n)\hat{\boldsymbol{s}}(n), \ldots, \boldsymbol{x}_{L_{\hat{s}}}^T(n - L_w + 1)\hat{\boldsymbol{s}}(n - L_w + 1)]^T$. If we assume that $\hat{\boldsymbol{s}}(n)$ is updated sufficiently slowly so that $\hat{\boldsymbol{s}}(n) \approx \hat{\boldsymbol{s}}(n-1) \approx \cdots \approx \hat{\boldsymbol{s}}(n - L_w + 1)$, then $\hat{\boldsymbol{x}}_s(n) \approx \boldsymbol{X}(n)\hat{\boldsymbol{s}}(n)$, where $\boldsymbol{X}(n) = [\boldsymbol{x}_{L_{\hat{s}}}(n), \ldots, \boldsymbol{x}_{L_{\hat{s}}}(n - L_w + 1)]^T$. Hence, $\boldsymbol{R}_{\hat{x}_s x_s}(n) \approx E[\boldsymbol{X}(n)\hat{\boldsymbol{s}}(n)\boldsymbol{s}\boldsymbol{X}^T(n)]$. Since the term $E[\hat{\boldsymbol{s}}(n)]$ converges to $\boldsymbol{s}$ asymptotically, $\boldsymbol{R}_{\hat{x}_s x_s}(n) \approx E[\boldsymbol{X}(n)\boldsymbol{s}\boldsymbol{s}^T\boldsymbol{X}^T(n)] \equiv \boldsymbol{R}_{x_s x_s}$, which is symmetric. Similarly, we have $\boldsymbol{r}_{\hat{x}_s x} \approx \boldsymbol{r}_{x_s x} = E[\boldsymbol{X}(n)\boldsymbol{s}\boldsymbol{x}_{L_p}^T(n)]$ for large n. Thus, $\boldsymbol{w}^* = -\boldsymbol{R}_{x_s x_s}^{-1}\boldsymbol{r}_{x_s x}\boldsymbol{p}$.

Let $\boldsymbol{\nu}_w(n) = \boldsymbol{w}^*(n) - \boldsymbol{w}(n)$ be the weight error vector, (3) can be rewritten as

$$\bar{\boldsymbol{\nu}}_w(n+1) = (\boldsymbol{I} - \mu_w \boldsymbol{R}_{\hat{x}_s x_s}(n))\,\bar{\boldsymbol{\nu}}_w(n) \tag{10}$$

where $\bar{\boldsymbol{\nu}}_w(n) = E[\boldsymbol{\nu}_w(n)]$. The stability of (10) is determined asymptotically by the eigenvalues of $\boldsymbol{R}_{x_s x_s}$. Let $\boldsymbol{U}\Lambda\boldsymbol{U}^T$ be the eigendecomposition of $\boldsymbol{R}_{x_s x_s}$, where $\boldsymbol{U}$ is an unitary matrix and $\Lambda = diag[\lambda_1, \ldots, \lambda_{L_w}]$ is a diagonal matrix containing eigenvalues of $\boldsymbol{R}_{x_s x_s}$. Therefore, the mean weight vector will converge if $|1 - \mu_w \lambda_{R_{x_s x_s},\max}| < 1$ or equivalently $0 < \mu_w < 2/\lambda_{R_{x_s x_s},\max}$, where $\lambda_{R_{x_s x_s},\max}$ is the maximum eigenvalue of $\boldsymbol{R}_{x_s x_s}$. It should be noted that when there is a step change in the system impulse response, the transient will decay with the slowness mode corresponding to the smallest eigenvalue above. In order to increase the tracking speed, variable step-size adaptive methods usually employ a larger step-size to damp down the transient first and gradually decrease its value to achieve a lower EMSE. The above step-size bound will serve as a guideline for choosing this maximum step-size.

B. Mean Square Convergence Analysis

Again, we shall analyze the mean square convergence performance of the secondary-path modeling and ANC in turn. Finally, the two results are used to analyze the steady-state behavior of the whole system.

1) Secondary-Path Adaptive Filter: Multiplying $\boldsymbol{\nu}_s(n)$ by its transpose and taking expectation on both sides of its updating equation, one gets a difference equation in the weight error covariance matrix $\Xi_s(\infty)E[\boldsymbol{\nu}_s(n)\boldsymbol{\nu}_s^T(n)]$ as follows:

$$\begin{aligned}\Xi_s(n+1) = \Xi_s(n) - \mu_s \boldsymbol{R}_{gg}\Xi_s(n) - \mu_s \Xi_s(n)\boldsymbol{R}_{gg} \\ + \mu_s^2 E[e_s^2(n)\boldsymbol{g}(n)\boldsymbol{g}^T(n)].\end{aligned} \tag{11}$$

The expectation of the last term above, $\boldsymbol{T}_s = E[e_s^2(n)\boldsymbol{g}(n)\boldsymbol{g}^T(n)]$, can be evaluated in Appendix A as

$$\begin{aligned}\boldsymbol{T}_s &= 2\boldsymbol{R}_{gg}\Xi_s(n)\boldsymbol{R}_{gg} + Tr(\boldsymbol{R}_{gg}\Xi_s(n) \\ &\quad + \boldsymbol{R}_{x_s x_s}\Xi_w(n))\boldsymbol{R}_{gg} + (\sigma_\eta^2 + \sigma_{\eta_w}^2(n))\boldsymbol{R}_{gg} \\ &\quad - 2E[\eta_w(n)\boldsymbol{x}_s^T(n)]\bar{\boldsymbol{\nu}}_w(n)\boldsymbol{R}_{gg}\end{aligned} \tag{12}$$

where $\Xi_w(n) = E[\boldsymbol{\nu}_w(n)\boldsymbol{\nu}_w^T(n)]$, $\eta_w(n) = \boldsymbol{p}^T\boldsymbol{x}_{L_p}(n) + \boldsymbol{x}_s^T(n)\boldsymbol{w}^*$ is the residual noise power, σ_η^2 and $\sigma_{\eta_w}^2$ are the variances of $\eta(n)$ and $\eta_w(n)$, respectively. Substituting (12) into (11) and noting that $\{g(n)\}$ is white, we get

$$\begin{aligned}\Xi_s(n+1) &= \Xi_s(n) - 2\mu_s\sigma_g^2\Xi_s(n) \\ &\quad + \mu_s^2\sigma_g^4(2\Xi_s(n) + Tr(\Xi_s(n)))\boldsymbol{I} \\ &\quad + \mu_s^2\{\sigma_\eta^2 + \sigma_M^2(n) - 2E[\eta_w(n)\boldsymbol{x}_s^T(n)]\bar{\boldsymbol{\nu}}_w(n)\}\sigma_g^2\boldsymbol{I}\end{aligned} \tag{13}$$

where $\sigma_M^2(n) = \sigma_{\eta_w}^2 + Tr(\boldsymbol{R}_{x_s x_s}\Xi_w(n))$.

It can be seen from (13) that the difference equation for the weight error covariance matrix of the secondary-path estimator is coupled with that of the ANC controller through the last driving term $\mu_s^2\{\sigma_\eta^2+\sigma_M^2(n)-2E[\eta_w(n)\boldsymbol{x}_s^T(n)]\bar{\boldsymbol{\nu}}_w(n)\}$. Note, since the coupling only affects the driving term, the stability behavior of (13) can be easily analyzed by treating it as an ordinary LMS algorithm [19], provided that the driving term is finite. Furthermore, the coupling effect due to the last driving term can be made smaller by using a smaller step-size μ_s and auxiliary noise power σ_g^2. Under this assumption, one gets the condition for stability to be

$$0 < \mu_s \leq \frac{2}{3Tr(\boldsymbol{R}_{gg})} = \frac{2}{3\sigma_g^2 L_s}. \tag{14}$$

Next, we wish to study the EMSE, which is defined as the additional or excess MSE over the minimum value achieved by the Wiener solution. It represents the additional MSE introduced due to the use of the LMS algorithm. It can be shown that for an adaptive filter with input $\boldsymbol{u}(n)$ and weight vector $\boldsymbol{w}(n)$ which converges in the mean to the Wiener solution, the EMSE at time instant n is equal to $Tr(\boldsymbol{R}_{uu}\Xi_w(n))$, where $\boldsymbol{R}_{uu}$ is the covariance matrix of $\boldsymbol{u}(n)$ and $\Xi_w(n)$ is the covariance of $\boldsymbol{w}(n)$. For the secondary-path adaptive estimator, the term $\bar{\boldsymbol{\nu}}_w(n)$ in (13) vanishes at the steady state. Hence, the steady-state EMSE can be derived from (13) as

$$\xi_s = Tr(\boldsymbol{R}_{gg}\Xi_s(\infty)) = \frac{\frac{1}{2}\mu_s(\sigma_\eta^2+\sigma_M^2(\infty))\phi_s}{1-\frac{1}{2}\mu_s\phi_s} \tag{15}$$

where $\phi_s = L_s\sigma_g^2/(1-\mu_s\sigma_g^2)$. The coupling term $\sigma_M^2(\infty)$ still needs to be determined, which will be presented after the analysis of the ANC controller. In addition, since the coupling effect has not been taking into account by assuming that the driving term is finite, (14) only serves as a maximum possible value of μ_s for achieving stability. A joint bound for the two step-sizes will be derived later at Section III-C, where the steady-state EMSE of the two coupled systems will be solved approximately.

2) FxLMS ANC Controller: For the ANC controller, the evolution equation of the covariance matrix $\Xi_w(n)$ can be similarly derived from (3) as (A-3) in Appendix B

$$\begin{aligned}\Xi_w(n+1) &= \Xi_w(n) \\ &\quad - \mu_w\{\Xi_w(n)\boldsymbol{R}_{x_s\hat{x}_s}(n) + \boldsymbol{R}_{\hat{x}_s x_s}(n)\Xi_w(n)\} \\ &\quad + \mu_w^2(\boldsymbol{T}_w(n)+\Delta_w(n))\end{aligned} \tag{16}$$

where $\Delta_w(n) = (\sigma_\eta^2 + \sigma_g^2 Tr(\boldsymbol{s}\boldsymbol{s}^T))\boldsymbol{R}_{\hat{x}_s\hat{x}_s}(n) + E[\eta_w^2(n)\hat{\boldsymbol{x}}_s(n)\hat{\boldsymbol{x}}_s^T(n)] - 2E[\eta_w(n)\hat{\boldsymbol{x}}_s(n)\boldsymbol{x}_s^T(n)\bar{\boldsymbol{\nu}}_w(n)\hat{\boldsymbol{x}}_s^T(n)]$ is the driving term and $\boldsymbol{T}_w(n) = E[\hat{\boldsymbol{x}}_s(n)\boldsymbol{x}_s^T(n)\Xi_w(n)\boldsymbol{x}_s(n)\hat{\boldsymbol{x}}_s^T(n)]$. Since (16) involves the expectation of several quantities with respect to the input, it can be rather difficult to obtain an explicit formula on the EMSE. To proceed further, we assume that the input is Gaussian distributed and evaluate the expectation on the right hand side of (16) using the Gaussian factoring theorem [18]. More precisely, the (i,j)-element of the term $\boldsymbol{T}_w(n)$ can be simplified to

$$\begin{aligned}&E[\hat{\boldsymbol{x}}_{s\_i}(n)\hat{\boldsymbol{x}}_{s\_j}(n)Tr(\Xi_w(n)\boldsymbol{x}_s(n)\boldsymbol{x}_s^T(n))] \\ &= E[\hat{\boldsymbol{x}}_{s\_i}(n)\hat{\boldsymbol{x}}_{s\_j}(n)]E[Tr(\Xi_w(n)\boldsymbol{x}_s(n)\boldsymbol{x}_s^T(n))] \\ &\quad + 2E[\hat{\boldsymbol{x}}_{s\_i}(n)\boldsymbol{x}_s^T(n)]\Xi_w(n)E[\boldsymbol{x}_s(n)\hat{\boldsymbol{x}}_{s\_j}(n)]\end{aligned}$$

where $\hat{\boldsymbol{x}}_{s\_k}(n)$ is the kth element of the vector $\hat{\boldsymbol{x}}_s(n)$. Thus,

$$\boldsymbol{T}_w(n) = Tr(\Xi_w(n)\boldsymbol{R}_{x_s x_s}(n))\boldsymbol{R}_{\hat{x}_s\hat{x}_s}(n) + 2\boldsymbol{R}_{\hat{x}_s x_s}(n)\Xi_w(n)\boldsymbol{R}_{x_s\hat{x}_s}(n).$$

By substituting the above result into (16), a difference equation describing the behavior of the ANC controller is obtained. Compared to the difference equation in (13), the secondary-path affects both the driving term and the system stability. On the other hand, the steady-state behavior can be studied by replacing $\boldsymbol{R}_{\hat{x}_s x_s}(n)$ in (16) with $\boldsymbol{R}_{x_s x_s}$, since $E[\hat{\boldsymbol{s}}(n)]$ converges quickly to $\boldsymbol{s}$ and $\boldsymbol{R}_{\hat{x}_s x_s}(n)\boldsymbol{R}_{x_s x_s}$. This gives for large n

$$\begin{aligned}\Xi_w(n+1) &= \Xi_w(n) - \mu_w\{\Xi_w(n)\boldsymbol{R}_{x_s x_s} + \boldsymbol{R}_{x_s x_s}\Xi_w(n)\} \\ &\quad + \mu_w^2\{E[\boldsymbol{x}_s(n)\boldsymbol{x}_s^T(n)\Xi_w(n)\boldsymbol{x}_s(n)\boldsymbol{x}_s^T(n)] \\ &\quad + E[\boldsymbol{X}(n)\Xi_s(n)\boldsymbol{X}^T(n)(\boldsymbol{s}^T\boldsymbol{X}^T(n)\Xi_w(n)\boldsymbol{X}(n)\boldsymbol{s})]\} \\ &\quad + \Delta_w(n)\}\end{aligned} \tag{17}$$

where we have used the fact that

$$\begin{aligned}\boldsymbol{T}_w(n) &= E\Big[\boldsymbol{X}(n)\hat{\boldsymbol{s}}(n)\boldsymbol{s}^T\boldsymbol{X}^T(n)\Xi_w(n)\boldsymbol{X}(n)\boldsymbol{s}\hat{\boldsymbol{s}}^T(n)\boldsymbol{X}^T(n)\Big] \\ &= E\Big[\boldsymbol{X}(n)(\boldsymbol{s}-\boldsymbol{\nu}_s(n))\boldsymbol{s}^T\boldsymbol{X}^T(n)\Xi_w(n)\boldsymbol{X}(n)\boldsymbol{s}(\boldsymbol{s}-\boldsymbol{\nu}_s(n))^T\boldsymbol{X}^T(n)\Big] \\ &= E\Big[\boldsymbol{X}(n)\boldsymbol{s}\boldsymbol{s}^T\boldsymbol{X}^T(n)\Xi_w(n)\boldsymbol{X}(n)\boldsymbol{s}\boldsymbol{s}^T\boldsymbol{X}^T(n)\Big] \\ &\quad + E\left[\boldsymbol{X}(n)\boldsymbol{\nu}_s(n)\boldsymbol{s}^T\boldsymbol{X}^T(n)\Xi_w(n)\boldsymbol{X}(n)\boldsymbol{s}\boldsymbol{\nu}_s^T(n)\boldsymbol{X}^T(n)\right] \\ &= E\Big[\boldsymbol{x}_s(n)\boldsymbol{x}_s^T(n)\Xi_w(n)\boldsymbol{x}_s(n)\boldsymbol{x}_s^T(n)\Big] \\ &\quad + E\left[\boldsymbol{X}(n)\boldsymbol{\nu}_s(n)\boldsymbol{s}^T\boldsymbol{X}^T(n)\Xi_w(n)\boldsymbol{X}(n)\boldsymbol{s}\boldsymbol{\nu}_s^T(n)\boldsymbol{X}^T(n)\right] \\ &= E\Big[\boldsymbol{x}_s(n)\boldsymbol{x}_s^T(n)\Xi_w(n)\boldsymbol{x}_s(n)\boldsymbol{x}_s^T(n)\Big] \\ &\quad + E\Big[\boldsymbol{X}(n)\boldsymbol{\nu}_s(n)\boldsymbol{\nu}_s^T(n)\boldsymbol{X}^T(n)\boldsymbol{s}^T\boldsymbol{X}^T(n)\Xi_w(n)\boldsymbol{X}(n)\boldsymbol{s}\Big]\end{aligned}$$

To study the stability of the difference equation for the ANC controller, we note that $\varphi_w(n) = Tr(\Xi_w(n))$ serves the role of the Lyapunov function which is always positive. Taking the trace on both sides of (17), one gets

$$\varphi_w(n+1) = \varphi_w(n)(1-r(n)) + \mu_w^2 Tr(\Delta_w(n))$$

where $r(n) = \left[2\mu_w Tr(\Xi_w(n)\boldsymbol{R}_{x_s x_s}) - \mu_w^2\gamma(n)\right]/\varphi_w(n)$ and

$$\begin{aligned}\gamma(n) &= Tr(E[\boldsymbol{X}(n)\hat{\boldsymbol{s}}(n)\boldsymbol{s}^T\boldsymbol{X}^T(n)\Xi_w(n)\boldsymbol{X}(n)\boldsymbol{s}\hat{s}^T(n)\boldsymbol{X}^T(n)]) \\ &\quad + Tr\left(E\left[\boldsymbol{X}(n)\Xi_s(n)\boldsymbol{X}^T(n)\boldsymbol{s}^T\boldsymbol{X}^T(n)\Xi_w(n)\boldsymbol{X}(n)\boldsymbol{s}\right]\right).\end{aligned}$$

For Gaussian inputs, the first term above can be written as $\gamma(n) = Tr(\Xi_w(n)\boldsymbol{R}_{x_s x_s})Tr(\boldsymbol{R}_{x_s x_s}) + 2Tr(\boldsymbol{R}_{x_s x_s}\Xi_w(n)\boldsymbol{R}_{x_s x_s})$. If the secondary path adaptive filter converges, then the driving term in $\mu_w^2 Tr(\Delta_w(n))$ in (16) and (17) will be finite. Since $\varphi_w(n)$ is positive, the system will be stable if

$$2\mu_w Tr(\Xi_w(n)\boldsymbol{R}_{x_s x_s}) - \mu_w^2\gamma(n) > 0$$

or equivalently:

$$\mu_w \leq \frac{2Tr(\Xi_w(n)\boldsymbol{R}_{x_s x_s})}{\gamma(n)} \equiv \mu_{w\_B}(n). \tag{18}$$

For a given probability density function (pdf) of $\boldsymbol{x}(n)$, one needs to evaluate $\gamma(n)$ in order to determine $\mu_{w\_B}(n)$. A simplification occurs when $\boldsymbol{x}(n)$ is Gaussian distributed and $\boldsymbol{X}(n)\Xi_s(n)\boldsymbol{X}^T(n)$ is weakly correlated with $\boldsymbol{s}^T\boldsymbol{X}^T(n)\Xi_w(n)\boldsymbol{X}(n)\boldsymbol{s}$. Then, using the inequality, $Tr(\boldsymbol{AB}) \leq Tr(\boldsymbol{A})Tr(\boldsymbol{B})$ for positive definite matrices $\boldsymbol{A}$ and $\boldsymbol{B}$, we have

$$\begin{aligned}
&Tr\big(E\big[\boldsymbol{X}(n)\Xi_s(n)\boldsymbol{X}^T(n)\boldsymbol{s}^T\boldsymbol{X}^T(n)\Xi_w(n)\boldsymbol{X}(n)\boldsymbol{s}\big]\big)\\
&\quad= E\big[Tr\big(\boldsymbol{X}(n)\Xi_s(n)\boldsymbol{X}^T(n)\boldsymbol{s}^T\boldsymbol{X}^T(n)\Xi_w(n)\boldsymbol{X}(n)\boldsymbol{s}\big)\big]\\
&\quad\geq E\big[Tr\big(\boldsymbol{X}(n)\Xi_s(n)\boldsymbol{X}^T(n)\cdot Tr(\boldsymbol{s}^T\boldsymbol{X}^T(n)\Xi_w(n)\boldsymbol{X}(n)\boldsymbol{s}\big)\big]\\
&\quad\approx E\big[Tr\big(\boldsymbol{X}(n)\Xi_s(n)\boldsymbol{X}^T(n)\big)\big]E\big[Tr\big(\boldsymbol{s}^T\boldsymbol{X}^T(n)\Xi_w(n)\boldsymbol{X}(n)\boldsymbol{s}\big)\big]\\
&\quad\approx Tr\big(E\big[\boldsymbol{X}(n)\Xi_s(n)\boldsymbol{X}^T(n)\big]\big)Tr\big(E\big[\boldsymbol{s}^T\boldsymbol{X}^T(n)\Xi_w(n)\boldsymbol{X}(n)\big]\big)
\end{aligned}$$

and $Tr(\boldsymbol{R}_{x_sx_s}\Xi_w(n)\boldsymbol{R}_{x_sx_s}) \leq Tr(\boldsymbol{R}_{x_sx_s}\Xi_w(n))Tr(\boldsymbol{R}_{x_sx_s})$. Thus, using this expression of $\gamma(n)$, (18) can be simplified to

$$\begin{aligned}
\mu_{w_B}(n) &\geq \frac{2}{3Tr(\boldsymbol{R}_{x_sx_s}) + Tr(E[\boldsymbol{X}(n)\Xi_s(n)\boldsymbol{X}^T(n)])}\\
&= \frac{2}{2Tr(\boldsymbol{R}_{x_sx_s}) + Tr(\boldsymbol{R}_{\hat{x}_s\hat{x}_s})}\\
&\geq \frac{2}{3Tr(\boldsymbol{R}_{\hat{x}_s\hat{x}_s})}
\end{aligned}$$

where we have used the fact that $E[\boldsymbol{x}_{\hat{s}}(n)\boldsymbol{x}_{\hat{s}}^T(n)] = \boldsymbol{R}_{x_sx_s} + E[\boldsymbol{X}(n)\Xi_s(n)\boldsymbol{X}^T(n)]$. Consequently, an approximate sufficient condition for $\boldsymbol{w}(n)$ to converge in the mean square sense is

$$\mu_w \leq \frac{2}{3Tr\left(\boldsymbol{R}_{\hat{x}_s\hat{x}_s}\right)}. \tag{19}$$

Equation (19) provides a useful bound for selecting the maximum step-size of μ_w. If variable step-size is used, this upper bound can be estimated online from the ensemble average of $Tr(\boldsymbol{R}_{\hat{x}_s\hat{x}_s})$ as $\hat{\sigma}^2_{\hat{x}_s\hat{x}_s}(n+1) = Tr(\hat{\boldsymbol{R}}_{\hat{x}_s\hat{x}_s}(n+1)) = \lambda Tr(\hat{\boldsymbol{R}}_{\hat{x}_s\hat{x}_s}(n)) + (1-\lambda)Tr(x_{\hat{s}}x_{\hat{s}}^T) = \lambda\hat{\sigma}^2_{\hat{x}_s\hat{x}_s}(n) + (1-\lambda)x_{\hat{s}}^Tx_{\hat{s}}$ using a forgetting factor λ. Similar to (14), (19) serves as a maximum possible value of μ_w for achieving stability. The joint effect of the two systems will be analyzed further at Section III-C.

Since both μ_w and μ_s are usually chosen as small values to achieve a low steady-state error, the term containing both $\Xi_s(n)$ and $\Xi_w(n)$ (i.e., the third term) on the right-hand side of (17) is usually small and can be neglected when studying the behavior near convergence. Using the following transformation $\boldsymbol{\Phi}(n) = \boldsymbol{U}^T\Xi_w(n)\boldsymbol{U}$:

$$\begin{aligned}
\Phi_{i,i}(n+1) \approx{}& \left(1 - 2\mu_w\lambda_i + 2\mu_w^2\lambda_i^2\right)\Phi_{i,i}(n)\\
&+ \mu_w^2 Tr\left(\boldsymbol{\Phi}(n)\Lambda\right)\lambda_i + \left(\boldsymbol{U}^T\Delta_w(n)\boldsymbol{U}\right)_{i,i}
\end{aligned} \tag{20}$$

where the subscript i,i denotes the (i,i)-element of the corresponding matrices.

At the steady state, $\Delta_w(\infty) = \mu_w^2\{(\sigma_\eta^2 + \sigma_g^2 Tr(\boldsymbol{ss}^T))\boldsymbol{R}_{\hat{x}_s\hat{x}_s}, +E[\eta_w^2(\infty)\hat{\boldsymbol{x}}_s(\infty)\hat{\boldsymbol{x}}_s^T(\infty)]\}$. Since the optimal residual $\eta_w(\infty)$ is weakly uncorrelated with $\hat{\boldsymbol{x}}_s(\infty)$, $E[\eta_w^2(\infty)\hat{\boldsymbol{x}}_s(\infty)\hat{\boldsymbol{x}}_s^T(\infty)]\} \approx E[\eta_w^2(\infty)]E[\hat{\boldsymbol{x}}_s(\infty)\hat{\boldsymbol{x}}_s^T(\infty)]\} = \sigma^2_{\eta_w}\boldsymbol{R}_{\hat{x}_s\hat{x}_s}(\infty)$ and hence,

$$\begin{aligned}
\boldsymbol{U}\Delta_w(\infty)\boldsymbol{U}^T &\approx \mu_w^2\left(\sigma_\eta^2 + \sigma_g^2 Tr(\boldsymbol{ss}^T) + \sigma^2_{\eta_w}\right)UR_{\hat{x}_s\hat{x}_s}\boldsymbol{U}^T\\
&= \mu_w^2\left(\sigma_\eta^2 + \sigma_g^2 Tr\left(\boldsymbol{ss}^T\right) + \sigma^2_{\eta_w}\right)\\
&\quad\times\left(\Lambda + \boldsymbol{U}E\left[\boldsymbol{X}(n)\Xi_s(\infty)\boldsymbol{X}^T(n)\right]\boldsymbol{U}^T\right)\\
&= \mu_w^2\sigma^2_{\min}\boldsymbol{D}\Lambda
\end{aligned} \tag{21}$$

where $\boldsymbol{D} = (\boldsymbol{I} + \boldsymbol{U}E[\boldsymbol{X}(n)\Xi_s(\infty)\boldsymbol{X}^T(n)]\boldsymbol{U}^T\Lambda^{-1})$ and $\sigma^2_{\min} = \sigma_\eta^2 + \sigma_g^2 Tr(\boldsymbol{ss}^T) + \sigma^2_{\eta_w}$.

Substituting (21) into (20) gives

$$\Phi_{i,i}(\infty) = \frac{\mu_w Tr(\boldsymbol{\Phi}(\infty)\Lambda) + \mu_w\sigma^2_{\min}d_{ii}}{2(1-\mu_w\lambda_i)} \tag{22}$$

where we have used the equality sign for simplicity and d_{ii} is the ith diagonal element of the matrix $\boldsymbol{D}$. The EMSE of $\boldsymbol{w}(n)$ is $\xi_w \equiv Tr(\Xi_w(\infty)\boldsymbol{R}_{x_sx_s}) = Tr(\Phi_w(\infty)\Lambda)$. Using (22), we have

$$\begin{aligned}
\xi_w &= \frac{\mu_w}{2}\left(Tr(\boldsymbol{\Phi}(\infty)\Lambda)\phi_{LMS} + \sigma^2_{\min}\phi_{D_LMS}\right)\\
&= \frac{\frac{1}{2}\mu_w\sigma^2_{\min}\phi_{D_LMS}}{1 - \frac{1}{2}\mu_w\phi_{LMS}}
\end{aligned} \tag{23}$$

where $\phi_{LMS} = \sum_{i=1}^{L_w}\lambda_i/(1-\mu_w\lambda_i)$ and $\phi_{D\_LMS} = \sum_{i=1}^{L_w}d_{ii}\lambda_i/(1-\mu_{w\lambda_i})$. For small μ_w

$$\begin{aligned}
\phi_{D_LMS} &\approx \sum_{i=1}^{L_w} d_{ii}\lambda_i\\
&= Tr(\boldsymbol{D}\Lambda)\\
&= Tr(\Lambda) + Tr(\Xi_s(\infty)E[\boldsymbol{X}^T(n)\boldsymbol{X}(n)])\\
&= Tr(\Lambda) + L_w Tr(\Xi_s(\infty)\boldsymbol{R}_{xx})
\end{aligned}$$

where we have used (21) and the independency of $\{\boldsymbol{x}(n)\}$ from assumption (A-1) in arriving at the second identity. Equation (23) is similar to the conventional LMS algorithm except for the term ϕ_{D_LMS}, which shows the coupling of the ANC controller with the secondary-path estimator through $\Xi_s(\infty)$.

Next, we shall combine the two steady-state results obtained in (15) and (23) above to solve the coupled equations for the steady-state MSE of the entire system at E, $E[\sigma_e^2(\infty)] = \overline{\sigma_e^2}(\infty)$. Moreover, due to the coupling, $\overline{\sigma_e^2}(\infty)$ is found to diverge if the product of the step-sizes of the ANC controller and secondary-path estimator is larger than a certain value. This gives an additional joint condition on μ_s and μ_w for achieving stability.

C. Steady-State MSE

From Fig. 1 and (5), the steady-state MSE is given by

$$E[\sigma_e^2(\infty)] = \sigma_M^2(\infty) + \sigma_g^2\boldsymbol{s}^T\boldsymbol{s} + \sigma_\eta^2 \tag{24}$$

where $\sigma_M^2(\infty)$ is defined in (13). Next, we shall evaluate $\sigma_M^2(\infty)$ by solving the coupled equations in (15) and (23) and utilize it to analyze the steady-state MSE of two commonly used noise injection methods depending on whether the noise variance is constant (Case2) or proportional to MSE (Case1).

First of all, we have from (23) that

$$\sigma_M^2(\infty) \approx \sigma_{\eta_w}^2 + \alpha_w \sigma_{\min}^2 [Tr(\Lambda) + L_w Tr(\Xi_s(\infty)\boldsymbol{R}_{xx})] \quad (25)$$

where $\alpha_w = \frac{1}{2}\mu_w/(1-\frac{1}{2}\mu_w \phi_{LMS})$. To simplify the analytical expression, we seek an upper bound of $\sigma_M^2(\infty)$ by noting that $Tr(\Xi_s(\infty)\boldsymbol{R}_{xx}) \le Tr(\Xi_s(\infty))Tr(\boldsymbol{R}_{xx})$. Consequently,

$$\begin{aligned}\sigma_M^2(\infty) &\le \sigma_{\eta_w}^2 + \alpha_w \sigma_{\min}^2 \left[Tr(\Lambda) + L_w Tr(\Xi_s(\infty))Tr(\boldsymbol{R}_{xx})\right] \\ &= \sigma_{\eta_w}^2 + \alpha_w \sigma_{\min}^2 \left[Tr(\Lambda) + L_w \xi_s(\infty)\sigma_g^{-2} Tr(\boldsymbol{R}_{xx})\right] \\ &= \sigma_{\eta_w}^2 + \alpha_w \sigma_{\min}^2 \left[Tr(\Lambda) + \alpha_s L_w L_s (\sigma_M^2(\infty) + \sigma_\eta^2) Tr(\boldsymbol{R}_{xx})\right]\end{aligned} \quad (26)$$

where $\alpha s = \frac{1}{2}\mu_s/(1-(1+\frac{1}{2}L_s)\mu_s\sigma_g^2)$ and we have used (15) for the derivation of the first equality above. Therefore, an upper bound of $\sigma_M^2(\infty)$ can be obtained by equating both sides of (26), which gives

$$\sigma_M^2(\infty) \le \frac{\sigma_{\eta_w}^2 + \alpha_w \sigma_{\min}^2 \phi}{1 - \alpha_w \alpha_s \sigma_{\min}^2 L_w L_s Tr(\boldsymbol{R}_{xx})} \quad (27)$$

where $\phi = Tr(\Lambda) + \alpha_s L_s L_w \sigma_\eta^2 Tr(\boldsymbol{R}_{xx})$. For simplicity, we shall use this upper bound as an estimate. Consequently, by substituting (27) into (15), an approximate EMSE for the secondary-path estimator in terms of σ_g^2 can be obtained. For Case 1, where the variance of injected noise σ_g^2 is proportional to $\overline{\sigma_e^2}(\infty)$, one will need to compute $\overline{\sigma_e^2}(\infty)$, whose analytical expression will be derived later in this section. It will be shown in the simulation results to be presented that this approximation gives good estimation of the EMSE values. Similarly, by using the same approximation above

$$Tr(\Xi_s(\infty)\boldsymbol{R}_{xx}) \le Tr(\Xi_s(\infty))Tr(\boldsymbol{R}_{xx}) = \xi_s(\infty)\sigma_g^{-2} Tr(\boldsymbol{R}_{xx})$$

one can get an upper bound of the EMSE of the ANC controller using (23) and the small step-size approximation $\phi_{D\_LMS} \approx Tr(\Lambda) + L_w Tr(\Xi_s(\infty)\boldsymbol{R}_{xx})$. This again depends on σ_g^2 and its computation will be similar to that described above.

Next, we consider two widely used systems with different choices of noise injection sequences $g(n)$: Case 1) $g(n) = g'(n)\hat{\sigma}_e(n-1)$ [11], [21] and Case 2) $g(n) = g'(n)$, where $g'(n)$ is a zero-mean white Gaussian sequence with variance $\sigma_{g'}^2$, $\hat{\sigma}_e^2(n-1) = \lambda\hat{\sigma}_e^2(n-2) + (1-\lambda)e^2(n-1)$ is the estimated residue noise power, and λ is a forgetting factor with $0 < \lambda < 1$. Following the discussion after (8), Case 1 usually leads to a faster convergence rate than Case 2 because the residual noise power is incorporated.

The steady-state MSEs are first derived and then the joint stability bounds of the ANC controller and secondary-path adaptive filter are analyzed. The difference equations of each subsystem determine their individual maximum possible values through (14) and (19). On the other hand, since the two subsystems are coupled together, their product needs to satisfy a joint stability condition as shown next.

Case 1) At the steady state, $\sigma_g^2(n) = E[g^2(n)] = E[(g'(n))^2]E[\hat{\sigma}_e^2(n-1)] = \sigma_{g'}^2 E[e^2(n-1)] = \sigma_{g'}^2\overline{\sigma_e^2}(n-1)$ for large n. Using the above expression for σ_g^2 and the upper bound of (27), one gets from (24) that

$$\overline{\sigma_e^2}(\infty) \approx \frac{\hat{\sigma}_\eta^2 + \alpha_w \sigma_{\min}^2 \left[Tr(\Lambda) + \alpha_s L_s L_w \sigma_\eta^2 Tr(\boldsymbol{R}_{xx})\right]}{1 - \alpha_s \alpha_w \sigma_{\min}^2 L_s L_w Tr(\boldsymbol{R}_{xx})} + \sigma_{g'}^2 \overline{\sigma_e^2}(\infty)\boldsymbol{s}^T\boldsymbol{s}$$

where $\hat{\sigma}_\eta^2 = \sigma_{\eta_w}^2 + \sigma_\eta^2 \left(1 - \alpha_s\alpha_w\sigma_{\min}^2 L_s L_w Tr(\boldsymbol{R}_{xx})\right)$ and $\overline{\sigma_e^2}$ denotes the estimated value of σ_e^2 by using the assumptions above. After some manipulation, we obtain

$$\overline{\sigma_e^2}(\infty) \approx \frac{\hat{\sigma}_\eta^2 + \alpha_w \sigma_{\min}^2 \left[Tr(\Lambda) + \alpha_s L_s L_w \sigma_\eta^2 Tr(\boldsymbol{R}_{xx})\right]}{(1 - \alpha_s \alpha_w \sigma_{\min}^2 L_s L_w Tr(\boldsymbol{R}_{xx}))\left(1 - \sigma_{g'}^2 \boldsymbol{s}^T\boldsymbol{s}\right)}. \quad (28)$$

It can be seen that $\overline{\sigma_e^2}(\infty)$ will be unbounded when $1 - \alpha_s\alpha_w\sigma_{\min}^2 L_s L_w Tr(\boldsymbol{R}_{xx}) = 0$ or $(1 - \sigma_{g'}^2\boldsymbol{s}^T\boldsymbol{s}) = 0$. The latter condition indicates that the injected noise variance has to be limited by $\sigma_{g'}^2 < (\boldsymbol{s}^T\boldsymbol{s})^{-1}$. Using the fact $\sigma_{\min}^2 = \sigma_\eta^2 + \sigma_g^2 Tr(\boldsymbol{s}\boldsymbol{s}^T) + \sigma_{\eta_w}^2$, the former suggests an upper bound for $\overline{\sigma_e^2}(\infty)$

$$\overline{\sigma_e^2}(\infty) < \frac{1}{Tr(\boldsymbol{s}\boldsymbol{s}^T)\sigma_{g'}^2}\left[(\alpha_s\alpha_w L_s L_w Tr(\boldsymbol{R}_{xx}))^{-1} - \sigma_{\eta\_\min}^2\right]$$

where $\sigma_{\eta\_\min}^2 = \sigma_\eta^2 + \sigma_{\eta_w}^2$. Consequently, the maximum possible injection noise power σ_g^2 is equal to

$$\begin{aligned}\sigma_{g\_\max}^2 &= \frac{\sigma_{g'}^2}{Tr(\boldsymbol{s}\boldsymbol{s}^T)\sigma_{g'}^2}\left[(\alpha_s\alpha_w L_s L_w Tr(\boldsymbol{R}_{xx}))^{-1} - \sigma_{\eta\_\min}^2\right] \\ &= \frac{1}{Tr(\boldsymbol{s}\boldsymbol{s}^T)}\left[\frac{1 - \sigma_{\eta\_\min}^2\alpha_s\alpha_w L_s L_w Tr(\boldsymbol{R}_{xx})}{\alpha_s\alpha_w L_s L_w Tr(\boldsymbol{R}_{xx})}\right]\end{aligned}$$

which has to be positive. It suggests $1 - \sigma_{\eta\_\min}^2\alpha_s\alpha_w L_s L_w Tr(\boldsymbol{R}_{xx}) > 0$, which after a slight manipulation becomes

$$\sigma_{g\_\max}^2 < \frac{1 - \frac{1}{2}\mu_s\sigma_{\eta\_\min}^2\alpha_w L_s L_w Tr(\boldsymbol{R}_{xx})}{\frac{1}{2}\mu_s(1+\frac{1}{2}L_s)}.$$

Again, we have $1 - 1/(2\mu_s\sigma_{\eta\_\min}^2\alpha_w L_s L_w Tr(\boldsymbol{R}_{xx})) > 0$ and hence $\mu_s < 2/(\sigma_{\eta\_\min}^2\alpha_w L_s L_w Tr(\boldsymbol{R}_{xx}))$. Combining with the bound on α_w in (19), denoted by $\alpha_{w\_\max}$, one has the following upper bound value for μ_s

$$\mu_{s\_\max} < \frac{2}{\sigma_{\eta\_\min}^2\alpha_{w\_\max} L_s L_w Tr(\boldsymbol{R}_{xx})}. \quad (29)$$

We also notice that (14) can be enforced by using the instantaneous value of $\sigma_{\min}^2$ computed and the minimum of this value or that calculated from (29) should be used, though it is expected that (29) will be smaller in general.

Since $\sigma_{\min}^2$ also depends on $\overline{\sigma_e^2}(\infty)$ through $\sigma_g^2 = \sigma_{g'}^2\overline{\sigma_e^2}(\infty)$, (28) is a highly nonlinear equation in

$\overline{\sigma_e^2}(\infty)$. To seek a closed-form expression of $\overline{\sigma_e^2}(\infty)$ for practical use, we take advantages of the commonly encountered small step-size situation to simplify further the denominator of (28). For notational convenience, let $r_s = 1-\sigma_{g'}^2 \boldsymbol{s}^T \boldsymbol{s}$. Then, by using binomial expansion of the denominator and retaining the first order term of $\overline{\sigma_e^2}(\infty)$ on the right-hand side, (28) becomes for small $\overline{\sigma_e^2}(\infty)$

$$\overline{\sigma_e^2}(\infty) \approx \frac{\hat{\sigma}_\eta^2 + \alpha_w \sigma_{\eta-\min}^2 \phi}{r_s - r_s \alpha_s \alpha_w \sigma_{\eta-\min}^2 L_s L_w Tr(\boldsymbol{R}_{xx}) - \alpha_w \sigma_{g'}^2 Tr(\boldsymbol{s}\boldsymbol{s}^T)\phi} \tag{30}$$

where $\hat{\sigma}_\eta^2 = \sigma_{\eta_w}^2 + \sigma_\eta^2(1 - \alpha_s \alpha_w \sigma_{\min}^2 L_s L_w Tr(\boldsymbol{R}_{xx}))$, $\sigma_{\eta-\min}^2 = \sigma_\eta^2 + \sigma_{\eta_w}^2$ are defined above, $\phi = Tr(\Lambda) + \alpha_s L_s L_w \sigma_\eta^2 Tr(\boldsymbol{R}_{xx})$ is defined in (27), and $\sigma_{\eta_w}^2$ is the minimum modeling error of the Wiener solution, which can be computed from $\boldsymbol{w}^*$ in (9) as $\sigma_{\eta_w}^2 = \boldsymbol{p}^T \left(\boldsymbol{R}_{xx} - \boldsymbol{r}_{x_s x}^T \boldsymbol{R}_{x_s x_s}^{-1} \boldsymbol{r}_{x_s x}\right) \boldsymbol{p}$. Quantities $\boldsymbol{r}_{x_s x} = E[\boldsymbol{X}(n)\boldsymbol{s}\boldsymbol{x}_{L_p}^T(n)]$ and $\boldsymbol{R}_{x_s x_s} = E[\boldsymbol{X}(n)\boldsymbol{s}\boldsymbol{s}^T \boldsymbol{X}^T(n)]$ can be computed using Monte Carlo simulation or from the given pdf of $\boldsymbol{x}(n)$.

We can also see from (30) that the approximate $\overline{\sigma_e^2}(\infty)$ will be unbounded if the denominator vanishes. This suggests that, other than the general upper bounds for the step-sizes in (14), (19), and (29), an approximate constraint on the product of the step-sizes of the ANC and secondary-path estimator should also be satisfied

$$1-\sigma_{g'}^2 \boldsymbol{s}^T \boldsymbol{s}\left(1 + \alpha_w \phi - \alpha_s \alpha_w \sigma_{\eta-\min}^2 L_s L_w Tr(\boldsymbol{R}_{xx})\right) - \alpha_s \alpha_w \sigma_{\eta-\min}^2 L_s L_w Tr(\boldsymbol{R}_{xx}) > 0 \tag{31}$$

to achieve stability. Simulation result shows that these bounds are reasonably tight. The details are omitted due to page limitation and are available from the authors upon request.

Case 2) Similar to the analysis in Case 1 and using the constant variance noise sequence $g(n) = g'(n)$, one can get from (24) and (27) that

$$\overline{\sigma_e^2}(\infty) \approx \frac{\hat{\sigma}_\eta^2 + \alpha_w \sigma_{\min}^2 \phi}{1 - \alpha_s \alpha_w \sigma_{\min}^2 L_s L_w Tr(\boldsymbol{R}_{xx})} + \sigma_g^2 \boldsymbol{s}^T \boldsymbol{s} \tag{32}$$

where $\sigma_{\min}^2 = \sigma_\eta^2 + \sigma_g^2 Tr(\boldsymbol{s}s^T) + \sigma_{\eta_w}^2$. Therefore, in Case 2, the following is required for stability other than the two general upper bounds in (14) and (19)

$$1 - \alpha_s \alpha_w \sigma_{\min}^2 L_s L_w Tr(\boldsymbol{R}_{xx}) > 0. \tag{33}$$

Due to the small step-sizes and other approximations used, it is found from simulation results that (33) somewhat overestimates the product of the two step-sizes within about one order of magnitude. A useful guideline is to divide the product of the step-sizes computed above by a factor of 10. On the other hand, the bounds in (14) and (19) are rather sharp in detecting instability. The use of these expressions in the design of ANC systems will be further illustrated in Example 3 in Section IV.

IV. Simulation Results

In this section, computer simulations are conducted to study the performance of the ANC system and verify the analytical results of its convergence behavior as discussed in Section III.

The following simulations are based on Eriksson's ANC structure in [6]. In experiments 1 and 2, simulation and theoretical results of the EMSE curves (Case 2) are compared for secondary paths with different lengths L_s. In experiment 3, the theoretical analysis derived is employed in an example design of an ANC controller for Case 2. In experiment 4, two practical ANC systems as described in Section III are compared.

The primary path is generated randomly as a FIR filter. The ANC system is supposed to be equipped in a small cabinet, say an automobile, and the noise source is close to the error microphone. Thus, a short primary path of length 12 is considered. The length of the controller $\boldsymbol{w}(n)$ is set to be 10, which is slightly shorter than that of the primary path. The background noise variance is $\sigma_\eta^2 = 0.04$. The auxiliary noise is a white Gaussian sequence with a variance $\sigma_g^2 = 0.2$ (Case 2). Both white and colored inputs are considered and their variances are normalized to be $\sigma_x^2 = 1$. For the colored input, a first order autoregressive (AR) process is considered and it is given by $x(n) = 0.9x(n-1) + v(n)$, where $v(n)$ is zero-mean and white Gaussian distributed. All simulation results are averaged over 200 Monte Carlo runs and the covariance matrix $\boldsymbol{R}_{xx}$ and other related quantities in computing the theoretical curves are estimated from the input signal by averaging over 1000 Monte Carlo runs.

A. Experiment 1: Sufficient-Order Secondary Path Modeling

In this experiment, the secondary path is assumed to be short and has a length of 8. Its estimator is also assumed to have a length of 8, i.e., the secondary path modeling is of sufficient order. In this experiment, the maximum step-sizes are calculated, respectively, to be 0.4 and 0.03, according to (14) and (19). The step-sizes are chosen within these bounds, which also satisfies (33). For both white and colored inputs $\{x(n)\}$, the step-size for the secondary-path estimator is identical and it is chosen as $\mu_s = 0.002$. For the ANC controller, the step-sizes for the white and colored inputs are, respectively, $\mu_w = 0.001$ and $\mu_w = 0.0005$. Fig. 2 shows the EMSE curves for both the ANC controller and the secondary-path estimator. It can be seen that the theoretical and simulated EMSE curves show the good agreement with each other. The transient behavior of the ANC controller is slightly underestimated by the theoretical analysis as shown in Fig. 2(b), since the last term of the difference equation (16), i.e., $2E[\eta_w(n)\hat{\boldsymbol{x}}_s(n)\boldsymbol{x}_s^T(n)\bar{\boldsymbol{\nu}}_w(n)\hat{\boldsymbol{x}}_s^T(n)]$, has been ignored in the derivation of theoretical results. Another possible reason is that, while the ANC controller converges at around the 5000th iteration, the secondary-path estimator has not yet converged. This results in the deviation between the simulation and theoretical results. The estimated steady-state EMSE values are

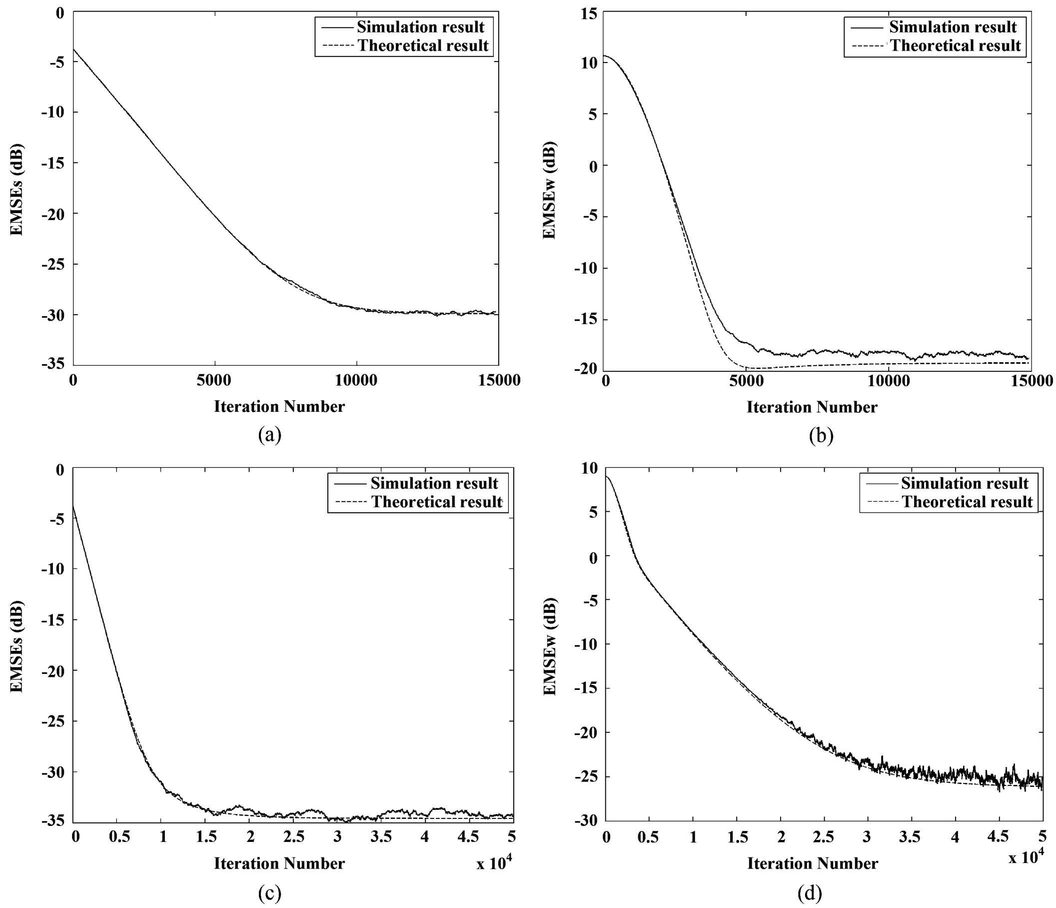

Fig. 2. Comparison of simulation and theoretical results of the EMSE curves with white Gaussian input for (a) the secondary path and (b) the ANC controller; and with the first-order AR process input for (c) the secondary path and (d) the ANC controller. $L_s = 8$. $\mu_s = 0.002$. $\mu_w = 0.001$ for the white input. $\mu_w = 0.0005$ for the colored input.

TABLE I
COMPARISON OF THE EXPERIMENTAL AND ESTIMATED STEADY-STATE EMSE FOR ANC CONTROLLER AND SECONDARY-PATH ESTIMATOR ($L_s = 8$)

SNR		SSS		LSS	
		EMSEs	EMSEw	EMSEs	EMSEw
WG	Simu	-29.8	-18.5	-22.6	-11.9
	Theo	-29.9	-19.1	-22.7	-12.8
AR	Simu	-34.5	-26.2	-29.9	-23.6
	Theo	-34.6	-26.4	-30.3	-24.1

Simu: simulation; Theo: theoretical; WG: white Gaussian; AR: autoregressive; EMSEw: steady-state EMSE of ANC controller; EMSEs: steady-state EMSE of secondary-path estimator; SSS: small step-size; LSS: large step-size.

compared with the simulation results in Table I (**SSS**), which also agree well with each other.

Next, we use comparatively larger step-sizes to evaluate the accuracy of the small step-size assumptions. For white input, $\mu_s = 0.01$ and $\mu_w = 0.004$ are evaluated. Whereas, for colored input, $\mu_s = 0.005$ and $\mu_w = 0.001$ are considered. Fig. 3 shows the simulated and the theoretically predicted EMSE curves. Again, the theoretical and simulated results also agree well with each other. Compared to the cases with smaller step-sizes, the transient behavior of the ANC controller has a slightly larger deviation from the theoretical results, as shown in Fig. 3(b), because the step-sizes are now much larger. The estimated steady-state EMSE values are also compared with the simulation results in Table I (**LSS**). It shows that the steady-state EMSE for the secondary path can be well estimated by the theoretical analysis, and similarly the estimated steady-state EMSE of the ANC controller slightly deviates from the true one (within 1 dB), despite the larger step-size used. Due to page limitation, results for the mean convergence analysis are omitted, which also agree well with the simulation results.

B. Experiment 2: Deficient-Order Secondary Path Modeling

In order to investigate the sensitivity of the mean square performance analysis in (13) to the modeling error of the secondary-path estimator, we consider the case $L_s > L_{\hat{s}}$ below. Simulations are conducted for a secondary path of length 50 which is to be estimated by an adaptive filter with a shorter length of 25. To make use of the analysis, we simply truncate the weight error vector in (13)–(15) to length 25. The step-size for the estimator is chosen as $\mu_s = 0.0015$. While for the ANC controller, the step-size is set to be $\mu_w = 0.001$ and $\mu_w = 0.0005$, respectively, for the white and colored inputs. Fig. 4 shows the convergence curves of EMSE and Table II shows the steady-state EMSE values of the simulated and theoretical results. It can be seen that the theoretical analyses can also model the transient and steady-state behaviors of the ANC system with long secondary path and deficient estimation order. Compared to Fig. 2(a) and (c) where the secondary path is short, the convergence speed of its estimator $\hat{\boldsymbol{s}}(n)$ becomes slower when the secondary path is longer. It can also be seen

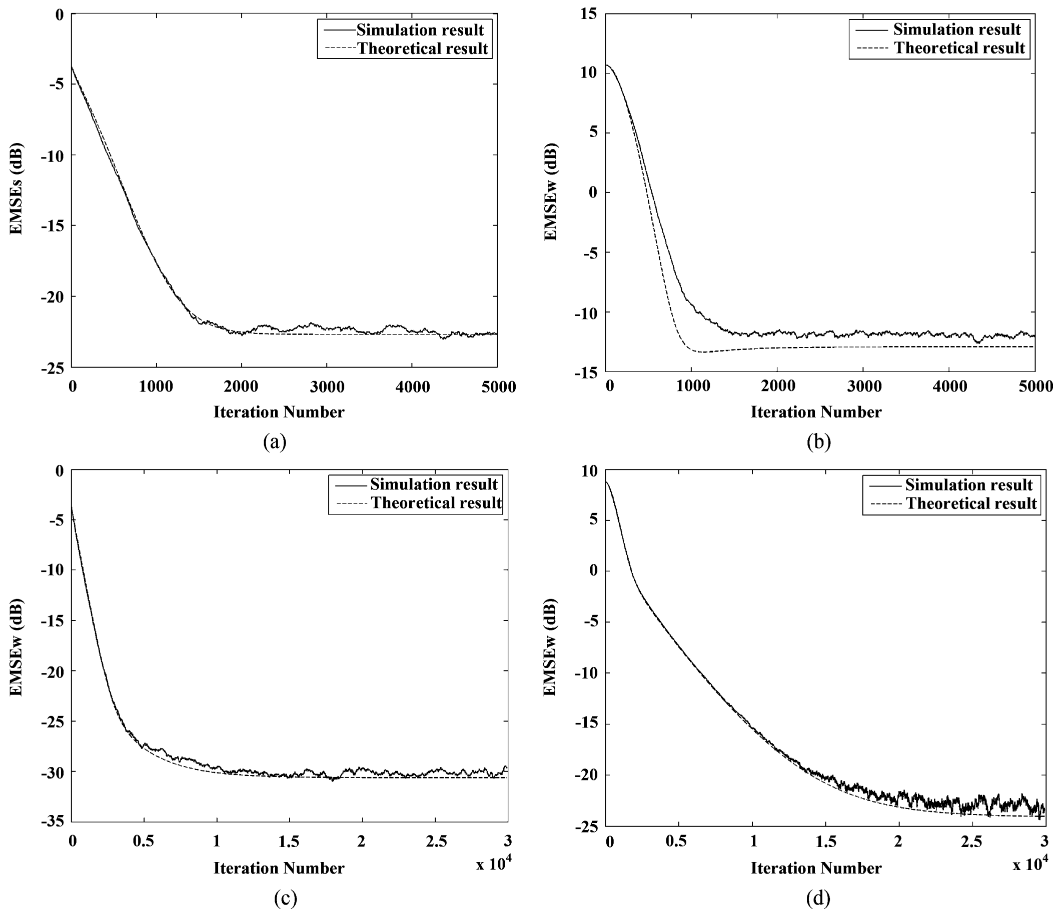

Fig. 3. Comparison of simulation and theoretical results of the EMSE curves with white Gaussian input for (a) the secondary path, (b) the ANC controller; and with the first-order AR process input for (c) the secondary path and (d) the ANC controller. $L_s = 8$. $\mu_s = 0.001$ and $\mu_w = 0.004$ for the white input. $\mu_s = 0.005$ and $\mu_w = 0.001$ for the colored input.

TABLE II
COMPARISON OF THE EXPERIMENTAL AND ESTIMATED STEADY-STATE EMSE FOR ANC CONTROLLER AND SECONDARY-PATH ESTIMATOR ($L_s = 50$)

SNR		SSS		LSS	
		EMSEs	EMSEw	EMSEs	EMSEw
WG	Simu	-24.6	-16.6	-21.5	-13.8
	Theo	-24.9	-17.7	-21.9	-15.3
AR	Simu	-30.0	-26.8	-26.6	-21.3
	Theo	-30.0	-26.9	-26.7	-21.6

Simu: simulation; Theo: theoretical; WG: white Gaussian; AR: autoregressive; EMSEw: steady-state EMSE of ANC controller; EMSEs: steady-state EMSE of secondary-path estimator; **SSS**: small step-size; **LSS**: large step-size.

that the steady-state EMSE of the secondary path becomes higher. This in turn affects the ANC controller due to their coupling effect. From the curves in Figs. 2 and 4 as well as the corresponding experimental data in Table II (**SSS**), it is observed that for the white input, the steady-state EMSE of the ANC controller, EMSEw, increases with the length of the secondary path, while for the colored input, EMSEw remains almost the same since a much smaller step-size μ_w is used and the coupling effect through the term σ_M^2 is small as shown in (27).

Next, we compare the estimated and simulated steady-state EMSE values by using comparatively larger step-sizes. For the white input, $\mu_s = 0.003$ and $\mu_w = 0.002$ are used while for the colored input, $\mu_s = 0.003$ and $\mu_w = 0.001$ are considered. The results are shown on the column **LSS** in Table II. It seems that compared to the results using small step-sizes, the deviation between theoretical estimation and simulation EMSE values increases slightly. The difference is within 1.5 dB.

C. Experiment 3: Design of a Case 2 ANC System

In this experiment, the proposed design procedure for ANC systems is derived from the theoretical analyses and its usefulness is illustrated by a design example. The settings are identical to that in Experiment 1 with colored input and the noise sequence $\{g(n)\}$ has constant variance (Case 2). Given the prior knowledge on the power of the input $\{x_s(n)\}$, the variances of $\{g(n)\}$ and $\{\eta(n)\}$ and the estimated variance of the modeling error $\sigma_{\eta_w}^2$, we shall determine the step-sizes for the ANC controller and the secondary-path estimator in order to achieve a desired steady- state EMSE for the controller ξ_w using the small step-sizes assumption. The proposed design procedure is summarized in Table III.

Suppose the power of the input $\{x_s(n)\}$ is 1.5 and the modeling error variance $\sigma_{\eta_w}^2$ is estimated to be 0.2, which has a mismatch with its true value $\sigma_{\eta_w}^2 = 0.19$ due to say channel length mismatch. The desired steady-state EMSE for the ANC controller is set to be $\xi_w = -23$ dB. First of all, $\sigma_{\min}^2$ can be calculated directly from (21) to be 0.7, where $\sigma_\eta^2 = 0.04$, $\sigma_g^2 = 0.2$ and $Tr(\boldsymbol{ss}^T) = 2.1$ (Step 1 in Table III). On the other hand, to achieve a good performance

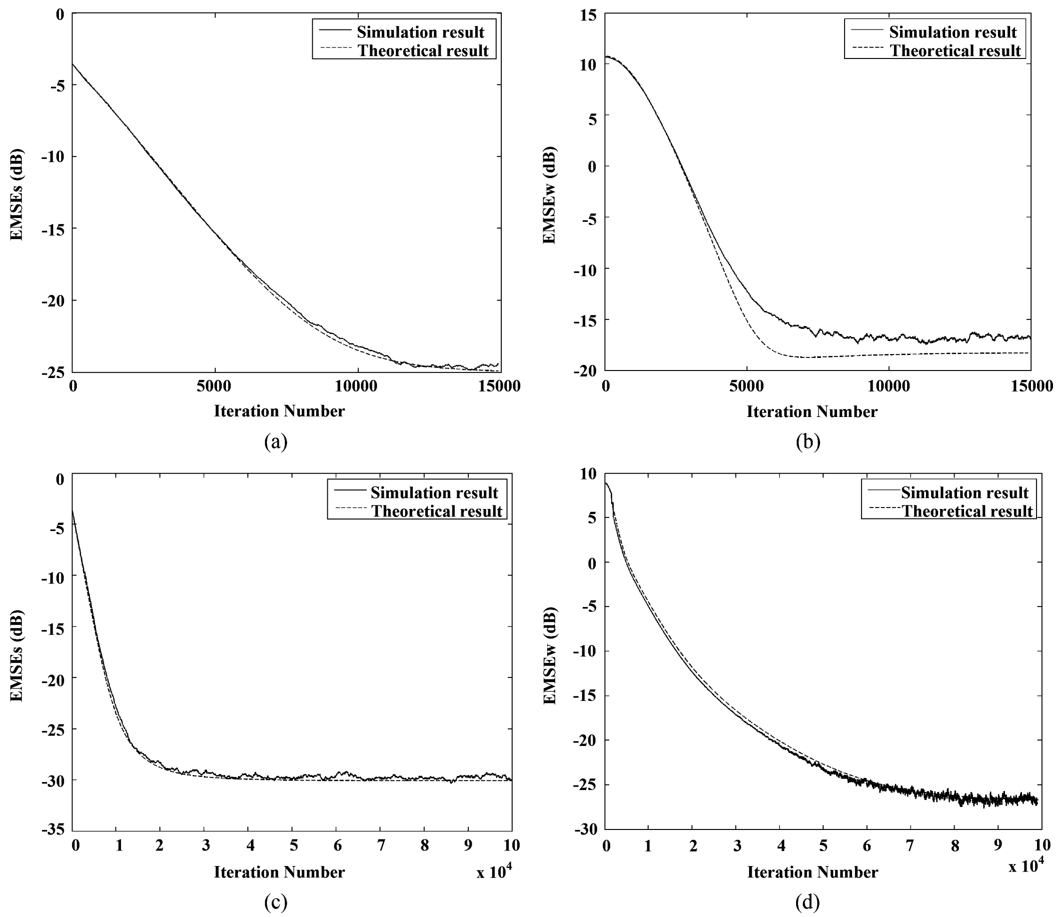

Fig. 4. Comparison of simulation and theoretical results of the EMSE curves with white Gaussian input for (a) the secondary path and (b) the ANC controller; and with the first-order AR process input for (c) the secondary path and (d) the ANC controller. $L_s = 50$. $\mu_s = 0.0015$. $\mu_w = 0.001$ for the white input. $\mu_w = 0.0005$ for the colored input.

TABLE III

PROPOSED DESIGN PROCEDURE FOR CASE2 SSS ANC SYSTEMS

Given the desired steady-state EMSE for the ANC controller, ξ_w, as well as the prior knowledge or estimate of the input power and noise variances, σ_η^2, σ_g^2 and $\sigma_{\eta_w}^2$.

Step 1 Calculate the step-size of the ANC controller μ_w from (23) using the small step size (SSS) approximation:

$$\mu_w \approx 2\xi_w / (\sigma_{\min}^2 \phi_{D\_LMS}),$$

where $\sigma_{\min}^2 = \sigma_\eta^2 + \sigma_g^2 Tr(\boldsymbol{ss}^T) + \sigma_{\eta_w}^2$ is defined in (21) and $\phi_{D\_LMS} = Tr(\Lambda) + L_w Tr(\Xi_s(\infty)\boldsymbol{R}_{xx})$ in (23) is chosen as $Tr(\Lambda)$ by design.

Step 2 Calculate the step-size of the secondary-path estimator μ_s from (15) using the SSS approximation as:

$$\mu_s \approx 2\xi_s / ((\sigma_\eta^2 + \sigma_M^2(\infty))\phi_s),$$

where $L_w Tr(\Xi_s(\infty)\boldsymbol{R}_{xx}) = 0.001 Tr(\Lambda)$ by design, $\xi_s = Tr(\Xi_s(\infty)\boldsymbol{R}_{xx}) \approx 0.001 Tr(\Lambda)/L_w$, and $\sigma_M^2(\infty) \approx \sigma_{\eta_w}^2$ (27) and $\phi_s \approx L_s \sigma_g^2$ (15) due to the SSS assumption.

Step 3 Check the stability conditions for the ANC controller and the secondary-path estimator in (14) and (19) and the extra stability constraint in (33). If these conditions are violated, a smaller ξ_w should be chosen.

we assume that a small step-size for the secondary-path estimator is used so that ϕ_{D_LMS} is approximately equal as $Tr(\Lambda) = 14.3$, since the other term $L_w Tr(\Xi_s(\infty)\boldsymbol{R}_{xx})$ is small compared to $Tr(\Lambda)$. Then, the step-size for the ANC controller can be calculated from (23). Since μ_w is usually very small, the term $1/(2\mu_w \phi_{LMS})$ in the denominator of (23) can be ignored to yield $\mu_w \approx 2\xi_w/(\sigma_{\min}^2 Tr(\Lambda)) \approx 0.001$. To determine the step-size for the secondary-path estimator, we assume that $L_w Tr(\Xi_s(\infty)\boldsymbol{R}_{xx})$ is a small portion of $Tr(\Lambda)$ as mentioned before, say 0.1% of $Tr(\Lambda)$. Thus, $\xi_s \approx 0.001 \cdot Tr(\Lambda)/L_w \approx 0.0015$ and by neglecting the small term $1/(2\mu_s\phi_s)$ in the denominator of (15), one gets $\mu_s \approx 2\xi_s(\infty)/((\sigma_\eta^2 + \sigma_M^2(\infty))\phi_s) \approx 0.007$ (Step 2). Finally, applying these two step-sizes to (14), (19), and (33), we found that the stability constraints are satisfied (Step 3). Using the two step-sizes in the ANC system, the obtained steady-state EMSE for the ANC controller is $\xi_w = -23.1$ dB, which is very close to the desired value of $\xi_w = -23$ dB. This illustrates the effectiveness of the proposed design procedure for ANC systems.

D. Experiment 4: Performance Comparison in Case 1 and 2

As described in Section III-C, two typical noise sequences $g(n)$ are usually used in ANC systems. In this experiment, the performances of these two noise sequence generation strategies are compared. The settings are the same as that in Experiment 1 and the input signal is a white Gaussian sequence. In Case 1, the noise sequence $g(n) = g'(n)\hat{\sigma}_e(n-1)$ with $\sigma_{g'}^2 = 0.01$ and

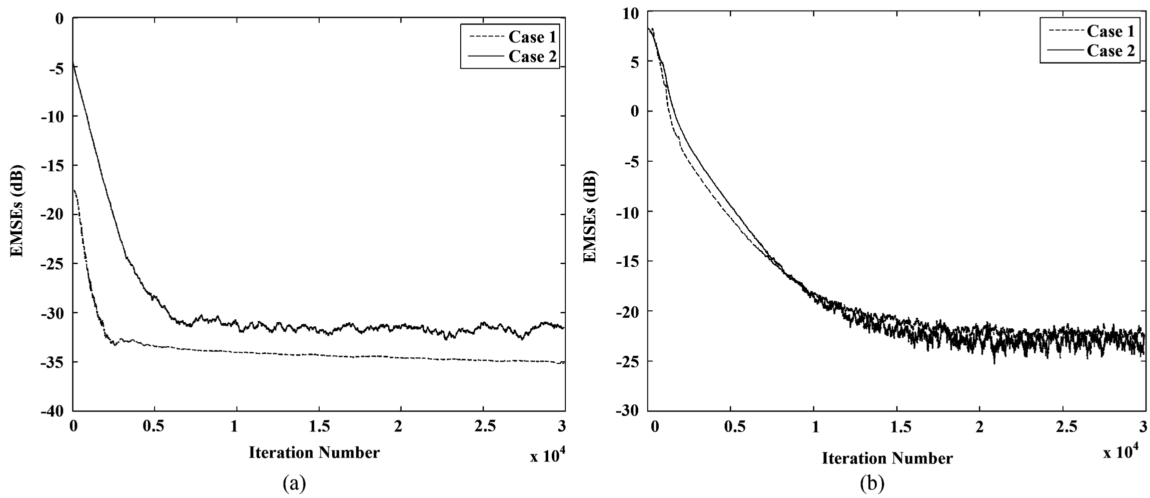

Fig. 5. Comparison of the EMSE curves in Case 1 and Case 2 with white Gaussian input for (a) the secondary path and (b) the ANC controller. $L_s = 8$. $\mu_w = 0.001$. $\mu_s = 0.02$ for Case 1. $\mu_s = 0.004$ for Case 2.

$\hat{\sigma}_e^2(n-1)$ is estimated by using a forgetting factor $\lambda = 0.999$ so that the correlation between $g(n)$ and $e(n)$ will be sufficiently small. In Case 2, $g(n) = g'(n)$ with $\sigma_g^2 = 0.2$. To obtain similar steady-state EMSE values for the two algorithms, the step-sizes $\mu_s = 0.02$ and $\mu_w = 0.001$ are used for Case 1, whereas $\mu_s = 0.004$ and $\mu_w = 0.001$ are used for Case 2. The simulation results are shown in Fig. 5. It can be seen in Fig. 5(a) that in Case 1, the secondary-path estimator converges at a much faster speed and to a lower steady-state value than that in Case 2. This agrees with the discussion in Section III-C, where a variable noise sequence is preferable. As for the ANC controller shown in Fig. 5(b), the convergence speed in Case 1 is slightly faster than that in Case 2 and the steady-state values are similar.

V. Conclusion

The mean and mean square convergence behaviors of FxLMS ANC systems with online secondary-path modeling have been presented. New difference equations describing the convergence behaviors of the ANC controller and the secondary-path estimator have been derived. Based on these difference equations, the stability of the system is analyzed and the steady-state EMSEs for the ANC controller and the secondary-path estimator are obtained. The analyses provide useful insight as well as guidance for the design and analyses of ANC systems with secondary-path modeling, which are illustrated with design examples. The simulation results are found to be in good agreement with the theoretical predictions.

Appendix A
Evaluation of $\boldsymbol{T}_S$

The expectation $T_s = E[e_s^2(n)\boldsymbol{g}(n)\boldsymbol{g}^T(n)]$ is now evaluated. First, we note from (6) that $e_s(n) = e_0(n) + \boldsymbol{\nu}_s^T\boldsymbol{g}(n)$. From (8), $e_0(n)$ can be rewritten as

$$\begin{aligned} e_0(n) &= (d(n) + \boldsymbol{x}_s^T(n)\boldsymbol{w}^*) \\ &\quad - \boldsymbol{x}_s^T(n)\boldsymbol{w}^* + \boldsymbol{x}_s^T(n)\boldsymbol{w}(n) \\ &= \eta_w(n) - \boldsymbol{x}_s^T(n)\boldsymbol{\nu}_w(n) + \eta(n) \end{aligned} \tag{A-1}$$

where $\eta_w(n) = \boldsymbol{p}^T\boldsymbol{x}_{L_p}(n) + \boldsymbol{x}_s^T(n)\boldsymbol{w}^*$ is the residual noise power of $x(n)$ at E for the optimal weight vector $\boldsymbol{w}^*$. Since $e_0(n)$ is independent of $\boldsymbol{g}(n)$, we obtain

$$\begin{aligned} \boldsymbol{T}_s &= E[\boldsymbol{g}(n)(\boldsymbol{g}^T(n)\Xi_s(n)\boldsymbol{g}(n) + e_0^2(n))\boldsymbol{g}^T(n)] \\ &= E[\boldsymbol{g}(n)\boldsymbol{g}^T(n)\Xi_s(n)\boldsymbol{g}(n)\boldsymbol{g}^T(n)] \\ &\quad + E[\boldsymbol{g}(n)\boldsymbol{x}_s^T(n)\Xi_w(n)\boldsymbol{x}_s(n)\boldsymbol{g}^T(n)] + (\sigma_\eta^2 + \sigma_{\eta_w}^2)\boldsymbol{R}_{gg} \\ &\quad - 2E[\eta_w(n)\boldsymbol{x}_s^T(n)]\bar{\boldsymbol{\nu}}_w(n)\boldsymbol{R}_{gg} \\ &= 2\boldsymbol{R}_{gg}\Xi_s(n)\boldsymbol{R}_{gg} + Tr(\boldsymbol{R}_{gg}\Xi_s(n) + \boldsymbol{R}_{x_sx_s}\Xi_w(n))\boldsymbol{R}_{gg} \\ &\quad + (\sigma_\eta^2 + \sigma_{\eta_w}^2(n))\boldsymbol{R}_{gg} - 2E[\eta_w(n)\boldsymbol{x}_s^T(n)]\bar{\boldsymbol{\nu}}_w(n)\boldsymbol{R}_{gg} \end{aligned} \tag{A-2}$$

where $\Xi_w(n) = E[\boldsymbol{\nu}_w(n)\boldsymbol{\nu}_w^T(n)]$, and σ_η^2 and $\sigma_{\eta_w}^2$ are the variances of $\eta(n)$ and $\eta_w(n)$, respectively. Note that in (A-2), we have used the Gaussian factoring theorem [18] to simplify the expression $E[\boldsymbol{g}(n)\boldsymbol{g}^T(n)\Xi_s(n)\boldsymbol{g}(n)\boldsymbol{g}^T(n)]$.

Appendix B
Derivation of the Difference Equation for Ξ_w

The difference equation for the ANC controller is now derived. From (5), we have $e(n) = e_0(n) + \boldsymbol{s}^T\boldsymbol{g}(n)$, where $e_0(n)$ has been rewritten as in (A-1). Multiplying $\boldsymbol{\nu}_w(n)$ by its transpose and taking expectation on both sides of the weight update equation, one gets from (3) the following:

$$\begin{aligned} \Xi_w(n+1) &= \Xi_w(n) - \mu_w E[e(n)(\boldsymbol{\nu}_w(n)\hat{\boldsymbol{x}}_s^T(n) \\ &\quad + \hat{\boldsymbol{x}}_s(n)\boldsymbol{\nu}_w^T(n))] + \mu_w^2 E[\hat{\boldsymbol{x}}_s(n)e^2(n)\boldsymbol{x}_s^T(n)] \\ &= \Xi_w(n) - \mu_w\{\Xi_w(n)\boldsymbol{R}_{x_s\hat{x}_s}(n) + \boldsymbol{R}_{\hat{x}_sx_s}(n)\Xi_w(n)\} \\ &\quad + \mu_w^2 E[\hat{\boldsymbol{x}}_s(n)(\boldsymbol{g}^T(n)\boldsymbol{s}\boldsymbol{s}^T\boldsymbol{g}(n) + e_0^2(n))\hat{\boldsymbol{x}}_s^T(n)] \\ &= \Xi_w(n) - \mu_w\{\Xi_w(n)\boldsymbol{R}_{x_s\hat{x}_s}(n) + \boldsymbol{R}_{\hat{x}_sx_s}(n)\Xi_w(n)\} \\ &\quad + \mu_w^2 E[\hat{\boldsymbol{x}}_s(n)\boldsymbol{x}_s^T(n)\Xi_w(n)\boldsymbol{x}_s(n)\hat{\boldsymbol{x}}_s^T(n)] \\ &\quad + \mu_w^2\Delta_w(n) \end{aligned} \tag{A-3}$$

where $\Delta_w(n) = (\sigma_\eta^2 + \sigma_g^2 Tr(\boldsymbol{s}\boldsymbol{s}^T))\boldsymbol{R}_{\hat{x}_s\hat{x}_s}(n) + E[\eta_w^2(n)\hat{\boldsymbol{x}}_s(n)\hat{\boldsymbol{x}}_s^T(n)] - 2E[\eta_w(n)\hat{\boldsymbol{x}}_s(n)\boldsymbol{x}_s^T(n)\bar{\boldsymbol{\nu}}_w(n)\hat{\boldsymbol{x}}_s^T(n)]$ is the driving term.

ACKNOWLEDGMENT

The authors would like to thank the reviewers for their constructive comments which greatly improve the presentation and technical content of the paper.

REFERENCES

[1] S. J. Elliott and P. A. Nelson, "Active noise control," *IEEE Signal Process. Mag*, vol. 10, no. 4, pp. 12–35, 1993.

[2] S. M. Kuo and D. R. Morgan, *Active Noise Control Systems—Algorithms and DSP Implementations*. New York: Wiley, 1996.

[3] P. A. Nelson and S. J. Elliotte, *Active Noise Control*. London, U. K.: Academic, 1995.

[4] D. R. Morgan, "An analysis of multiple correlation cancellation loops with a filter in the auxiliary path," *IEEE Trans. Acoust., Speech, Signal Process.*, vol. ASSP-28, no. 4, pp. 454–467, Aug. 1980.

[5] B. Widrow and S. D. Stearns, *Adaptive Signal Processing*. Englewood Cliffs, NJ: Prentice-Hall, 1985.

[6] L. J. Eriksson and M. C. Allie, "System considerations for adaptive modeling applied to active noise control," in *Proc. Int. Symp. Circuits Syst.*, 1988, vol. 3, pp. 2387–2390.

[7] C. Bao, P. Sas, and H. V. Brussel, "Adaptive active noise control of noise in 3-D reverberant enclosure," *J. Sound Vibr.*, vol. 161, no. 3, pp. 501–514, Mar. 1993.

[8] S. M. Kuo and M. J. Ji, "Development and analysis of an adaptive noise equalizer," *IEEE Trans. Speech Audio Process.*, vol. 3, no. 3, pp. 217–222, May 1995.

[9] S. M. Kuo and D. Vijayan, "A secondary-path modeling technique for active noise control systems," *IEEE Trans. Speech, Audio Process*, vol. 5, no. 4, pp. 374–377, Jul. 1997.

[10] M. Zhang, H. Lan, and W. Ser, "Cross-updated active noise control system with online secondary-path modeling," *IEEE Trans. Speech Audio Process.*, vol. 9, no. 5, pp. 598–602, Jul. 2001.

[11] H. Lan, M. Zhang, and W. Ser, "An active noise control system using online secondary-path modeling with reduced auxiliary noise," *IEEE Signal Process. Lett*, vol. 9, no. 1, pp. 16–18, Jan. 2002.

[12] M. Wu, X. Qiu, and G. Chen, "The statistical behavior of phase error for deficient-order secondary path modeling," *IEEE Signal Process. Lett*, vol. 15, pp. 313–316, 2008.

[13] Y. Xiao, L. Ma, and K. Hasegawa, "Properties of FXLMS-based narrowband active noise control with online secondary-path modeling," *IEEE Trans. Signal Process.*, vol. 57, no. 8, pp. 2931–2949, Aug. 2009.

[14] J. Liu, Y. Xiao, J. Sun, and L. Xu, "Analysis of online secondary-path modeling with auxiliary noise scaled by residual noise signal," *IEEE Trans. Audio, Speech, Lang. Process.*, vol. 18, no. 8, pp. 1978–1993, Nov. 2010.

[15] M. Zhang, H. Lan, and W. Ser, "On comparison of online secondary path modeling methods with auxiliary noise," *IEEE Trans. Speech Audio Process.*, vol. 13, no. 4, pp. 618–628, Jul. 2005.

[16] B. Widrow, J. M. McCool, M. G. Larimore, and C. R. Johnson, "Stationary and nonstationary learning characteristics of the LMS adaptive filter," *Proc. IEEE*, vol. 64, no. 8, pp. 2931–2949, Aug. 1976.

[17] M. T. Akhtar, M. Abe, and M. Kawamata, "A new variable step size LMS algorithm-based method for improved online secondary-path modeling in active noise control systems," *IEEE Trans. Audio, Speech, Lang. Process.*, vol. 14, no. 2, pp. 720–726, Mar. 2006.

[18] R. H. Kwong and E. W. Johnston, "A variable step size LMS algorithm," *IEEE Trans. Signal Process.*, vol. 40, no. 7, pp. 1633–1642, Jul. 1992.

[19] S. Haykin, *Adaptive Filter Theory*. Englewood Cliffs, NJ: Prentice-Hall, 1996.

[20] B. Widrow and S. D. Stearns, *Adaptive Signal Processing*. Englewood Cliffs, NJ: Prentice-Hall, 1985.

[21] D. Cornelissen and P. C. W. Sommen, "New online secondary path estimation in a multipoint filtered-X algorithm for acoustic noise canceling," in *Proc. IEEE ProRIS 99*, 1999, pp. 97–103.

Shing Chow Chan (S'87–M'92) received the B.Sc. (Eng.) and Ph.D. degrees from The University of Hong Kong, Pokfulam, Hong Kong, in 1986 and 1992, respectively.

In 1990, he was with the City Polytechnic of Hong Kong, Kowloon, Hong Kong, where he was an Assistant Lecturer and, later, a University Lecturer. Since 1994, he has been with the Department of Electrical and Electronic Engineering, The University of Hong Kong, where he is currently a Professor. He was a Visiting Researcher with Microsoft Corporation, Redmond, WA, Microsoft, Beijing, China, University of Texas at Arlington, Arlington, and Nanyang Technological University, Singapore. His research interests include fast transform algorithms, filter design and realization, multirate and biomedical signal processing, communications and array signal processing, high-speed A-D converter architecture, bioinformatics, and image-based rendering.

Dr. Chan is currently a member of the Digital Signal Processing Technical Committee of the IEEE Circuits and Systems Society and an Associate Editor of the Journal of Signal Processing Systems. He was the Chairman of the IEEE Hong Kong Chapter of Signal Processing in 2000–2002, an organizing committee member of the IEEE International Conference on Acoustics, Speech, and Signal Processing 2003 and the International Conference on Image Processing 2010, and an Associate Editor of the IEEE TRANSACTIONS ON CIRCUITS AND SYSTEMS I in 2008–2009.

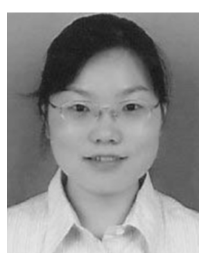

Yijing Chu received the B.S. and M.S. degree in acoustics from the Nanjing University, Nanjing, China, in 2005 and 2008, respectively. She is currently working towards the Ph.D. degree with the Electrical and Electronics Engineering Department, The University of Hong Kong, Hong Kong, SAR.

In 2006, she served as a Research Assistant in the Department of Building Service Engineering, Polytechnic University of Hong Kong, Hong Kong. Her current research interest is the analysis, design and applications of robust adaptive filtering algorithms.